Assessment of MJO Predictability for Boreal Winter with Various Statistical and Dynamical Models

IN-SIK KANG

School of Earth and Environmental Sciences, Seoul National University, Seoul, South Korea

HYE-MI KIM

School of Earth and Atmospheric Science, Georgia Institute of Technology, Atlanta, Georgia

(Manuscript received 12 June 2009, in final form 21 December 2009)

ABSTRACT

The predictability of intraseasonal variation in the tropics is assessed in the present study by using various statistical and dynamical models with rigorous and fair measurements. For a fair comparison, the real-time multivariate Madden–Julian oscillation (MJO) (RMM) index, proposed by Wheeler and Hendon, is used as a predictand for all models. The statistical models include the models based on a multilinear regression, a wavelet analysis, and a singular spectrum analysis (SSA). The prediction limits (correlation skill of 0.5) of statistical models for RMM1 (RMM2) index are at days 16–17 (14–15) for the multiregression model, whereas they are at days 8–10 (9–12) for the wavelet- and SSA-based models. The poor predictability of the wavelet and SSA models is related to the tapering problem for a half-length of the time window before the initial condition.

To assess the dynamical predictability, long-term serial prediction experiments with a prediction interval of every 5 days are carried out with Seoul National University (SNU) AGCM and coupled general circulation model (CGCM) for 26 (1980–2005) boreal winters. The prediction limits of RMM1 and RMM2 occur at around 20 days for both AGCM and CGCM. These results demonstrate that the skills of dynamical models used in this study are better than those of the three statistical predictions. The dynamical and statistical predictions are combined using a multimodel ensemble method. The combination provides a superior skill to any of the statistical and dynamical predictions, with a prediction limit of 22–24 days. The dependencies of prediction skill on the initial phase and amplitude of the MJO are also investigated.

1. Introduction

In recent years, there have been a lot of demands from society for extended forecasts with time scales longer than weeks, particularly predictions of rainy and dry periods within a season. For those predictions, we need a prediction system that provides information on the subseasonal variations. Several statistical models have been developed for the subseasonal prediction, and those statistical models appear to have a predictability time scale of a few weeks (Waliser et al. 1999a; Lo and Hendon 2000; Mo 2001; Jones et al. 2004; Webster and Hoyos 2004; Maharaj and Wheeler 2005; Jiang et al. 2008), whereas the dynamical prediction has been limited mainly because of poor simulations of intraseasonal variations. Previous studies indicate that the dynamical predictability appears to be about 7–10 days (Chen and Alpert 1990; Lau and Chang 1992; Schemm et al. 1996; Hendon et al. 2000; Jones et al. 2000; Seo et al. 2005). But, it should be pointed out that those previous studies have used different predictands and different periods for their prediction experiments, so that one has difficulty determining the prediction skills for the variables selected for one's own purpose and selecting the best method/model for the Madden–Julian oscillation (MJO) prediction.

For last decades, a number of research studies have been carried out to understand and simulate the MJO, which controls most of the variance of subseasonal variations in the tropical monsoon region. Several MJO intercomparison projects of the atmospheric general circulation model (AGCM) have been performed (Slingo et al. 1996;

Corresponding author address: In-Sik Kang, School of Earth and Environmental Sciences, Seoul National University, Seoul 151-742, South Korea.
E-mail: kang@climate.snu.ac.kr

DOI: 10.1175/2010JCLI3288.1

Kang et al. 2002; Wu et al. 2002; Waliser et al. 2003) and those studies have shown that the AGCM capability of simulating MJO has a limitation but has been continuously improved. Several recent studies showed that the air–sea coupling process is an important mechanism for the maintenance and propagation of MJO (Waliser et al. 1999b; Woolnough et al. 2000; Webster et al. 2002; Fu et al. 2003; Fu and Wang 2004a,b; Rajendran et al. 2004), and recent ocean–atmosphere coupled GCMs (CGCMs) are shown to simulate the MJO better than those recent AGCMs (Zheng et al. 2004; Rajendran and Kitoh 2006; Fu et al. 2007; Kim et al. 2010). It would be natural to use those models for subseasonal and MJO predictions. A few attempts have been made and reported in recent years (Woolnough et al. 2007; Vitart et al. 2007). But, those studies have limited assess to MJO predictability mainly because of a limited period of prediction experiments. It is also pointed out that the predictability depends on the model, and the assessment of predictability should be continuously updated with improvement of the model and by using various different models.

The statistical prediction models have been developed using various methods, based on a regression using empirical orthogonal function (EOF; Lo and Hendon 2000; Goswami and Xavier 2003; Jones et al. 2004; Jiang et al. 2008), singular spectrum analysis (Mo 2001), wavelet analysis (Webster and Hoyos 2004), and neural network models (Love and Matthews 2009). To rigorously assess the predictability of those statistical models, we have developed those models independently and examined the MJO predictability based on the same prediction framework. The dynamical models used in this study include AGCM and CGCM, which have been developed at Seoul National University (SNU) and used in various modeling works and prediction experiments (Kim et al. 1998; Kang et al. 2002; Waliser et al. 2003; Kug et al. 2007; Kim and Kang 2008; Kim et al. 2008a,b; and many others). We adapted the same framework of prediction for both statistical and dynamical predictions, such as for the period, internal of prediction, and predictands. The predictands used in the present study are the MJO indices developed by Wheeler and Hendon (2004, hereafter WH04), which are now being used in monitoring and predicting MJO in a real-time basis at various operational centers, such as the National Centers for Environmental Prediction (NCEP).

The aims of the present study include 1) rigorously assessing the MJO predictability of the statistical and dynamical models currently available, 2) developing an optimum prediction system for MJO by combining the statistical and dynamical models, and 3) understanding the limitations of MJO prediction in the statistical and dynamical models. Section 2 introduces details of the statistical models used in the present study and assesses the MJO predictability of the statistical model. Section 3 examines the MJO predictability of the AGCM and CGCM. Section 4 combines the statistical model and dynamical model predictions, and section 5 examines MJO predictability on the initial amplitude and phase. The summary and concluding remarks are given in section 6.

2. Predictability of various statistical models

All the prediction models here are developed to predict the real-time multivariate Madden–Julian oscillation (RMM) indices. The RMM indices are the time series associated with the first (RMM1) and second (RMM2) eigenvectors of the combined EOF of the outgoing longwave radiation (OLR) and zonal wind fields at 200 and 850 hPa over the tropical belt, averaged between 15°S and 15°N after removing only the interannual variability (WH04). Although the three variables are used without any time filtering process, the leading eigenmodes and associated time series represent the MJO reasonably well (WH04; Kim 2008). The observation data used in the present study are obtained from the NCEP reanalysis dataset for 27 winter months [November–March (NDJFM)] from 1979/80 to 2005/06.

a. Multilinear regression model

A multilinear regression (MREG) model is constructed to predict the RMM indices, which can be written as

$$X(t_0 + \tau) = \sum_{p=1}^{m} \sum_{j=1}^{\lambda} B_{pj}(\tau) X_p(t_0 - j + 1), \qquad (1)$$

where X is the RMM index, t_0 is the initial time point, and τ is the forecast lead time. Here m is the number of total modes (RMM1 and RMM2) and λ is the number of lagged days before the prediction. The B_{pj} is the lag-regression parameter for X at j^{th} day before the initial time t_0. For the purpose of ''real time'' application, a cross-validation method (leave one year out) is applied to obtain the regression parameters B_{pj}. We examined the sensitivity of the prediction skill by increasing the lag λ and mode m (Kim 2008). The results demonstrate that inclusion of additional lags or modes does not change much of the prediction skill. Based on the sensitivity test, the forecast model uses $m = 2$ and $\lambda = 2$. Figure 1 shows the prediction skill of RMMs using the MREG model. The correlation decreases to 0.5 after day 16–17 (day 14–15) for RMM1 (RMM2).

The spatial distributions of predicted OLR anomalies are obtained by using the predicted RMM1 and RMM2

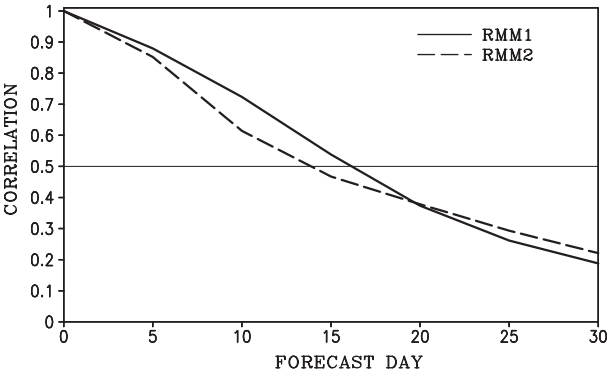

FIG. 1. Correlation skill of MREG models for RMM1 (solid line) and RMM2 (dashed line) indices as a function of forecast lead time.

and the associated OLR anomaly patterns. The following formula is used for reconstructing the OLR anomalies:

$$\text{R-OLR}(x, y, t_0 + \tau) = X_1(x, y)\text{RMM1}(t_0 + \tau) + X_2\text{RMM2}(t_0 + \tau),$$

where R-OLR is the reconstructed OLR anomaly and X is the regressed OLR anomaly pattern onto RMM1 and RMM2. Figure 2 shows the spatial distribution of correlation skill between the predicted OLR and the observed counterpart. A relatively high correlation skill is seen in the equatorial Indian Ocean and the western Pacific Ocean. Those regions coincide with the area of largest MJO variability. Even though the present study uses the unfiltered OLR, the prediction skills over the tropical region are as high as 0.3 for day 15. Similar results are also obtained by Jiang et al. (2008).

b. *Wavelet-based prediction*

Using the method of Torrence and Compo (1998), the original time series are reconstructed in terms of a family of wavelet transforms. The reconstructed time series can be constructed as the sum of the real part of the wavelet transforms. In this study, we forecast the real part of each spectral band using the auto linear regression method and then reconstructed the predicted time series using the sum of the predicted real parts of each spectral band. The cross validation is also applied in this real-time prediction, in which the regression coefficients are obtained by using the data without the winter period of the target year to be predicted.

Because one is dealing with a finite-length time series, errors occur at the beginning and end points of the wavelet power spectrum (Torrence and Compo 1998). This is a critical problem in real-time prediction because the information just before the initial condition is the most important values for the prediction. The solution adapted in this study is to taper the end of the time series before

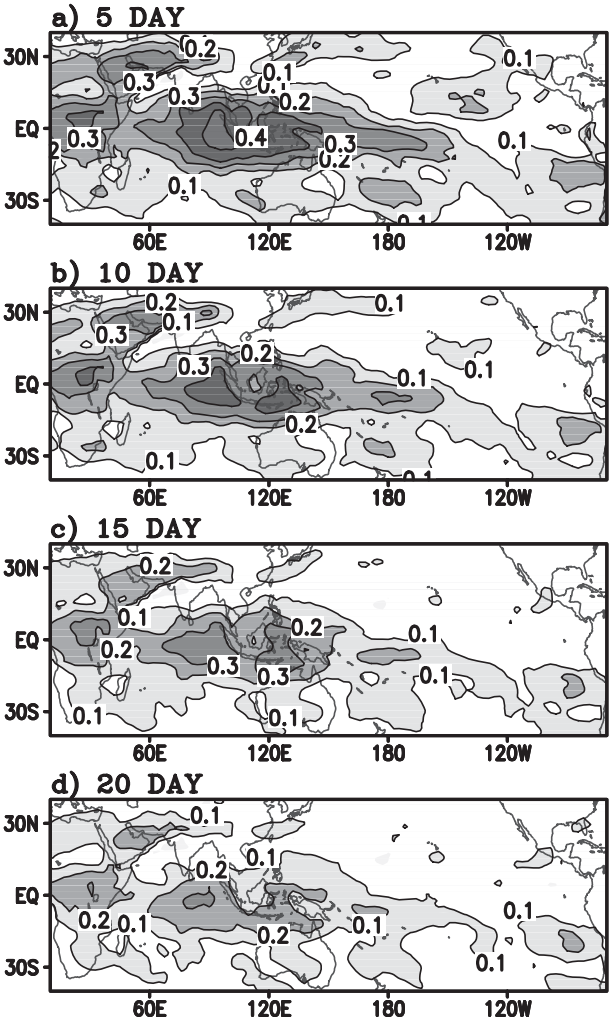

FIG. 2. Distribution of correlation coefficients between predicted and observed OLR anomalies for lead times from (a) 5 to (d) 20 days. Contour interval is 0.1.

doing the wavelet transform using a cosine damping proposed by Meyers et al. (1993). As mentioned earlier, the wavelet method makes the predictions of each spectral bands, whose prediction skills are shown in Fig. 3. The figure shows the prediction skill of each spectral band of RMM1 as a function of lead time. The correlation has a relatively high value on the spectral bands of 30–80 days where the RMMs have strong variances. In those spectral bands, the correlation skill shows more than 0.6 after a 30-day lead time. However, the high-frequency bands are unpredictable even at the beginning of the prediction. Higher frequencies are more difficult to predict than the low frequencies, since the edge effects are more severe for the higher frequencies. The prediction for a certain spectral domain can be obtained by the sum of predictions of spectral bands within the domain. Figure 4

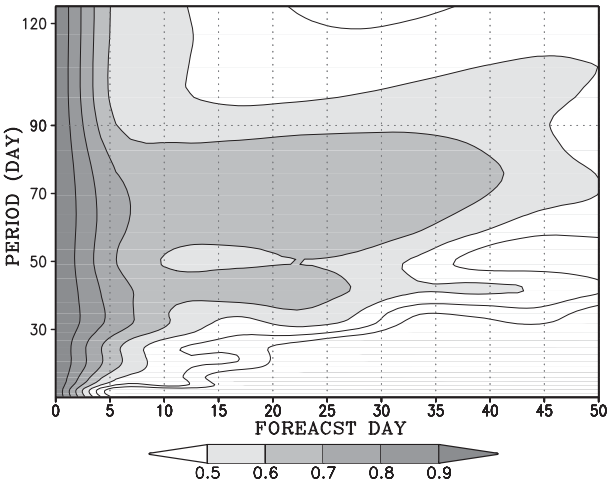

FIG. 3. Correlation skill of the wavelet-based model. Plotted is the correlation coefficient between the predicted and observed RMM1 time series for individual wavelet bands as a function of forecast lead time.

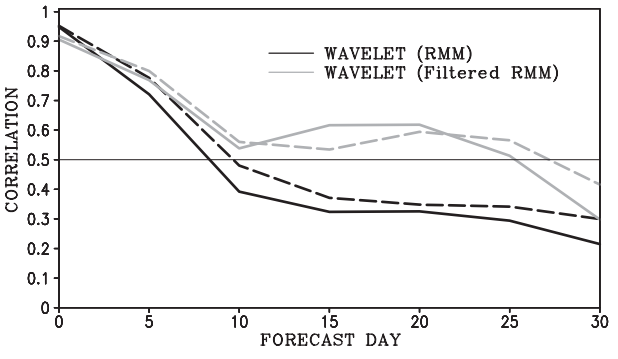

FIG. 4. Correlation coefficients of the wavelet-based predicted and observed RMM1 (solid line) and RMM2 (dashed line) for the total unfiltered data (black) and 30–80-day filtered data (gray).

shows the prediction skill of the time series of RMM1 (solid line) and RMM2 (dashed line) for a spectral domain of 30–80 days (gray lines) and for a total field (black lines). Clearly, the wavelet-based model has a limitation for predicting the total fields but provides a good prediction skill with the prediction limit of more than 25 days when the prediction is confined to the intraseasonal time scales. The increase of predictability after 10 days in the filtered RMM index might result from the high predictability of low-frequency variations.

c. *SSA-based prediction*

Singular spectrum analysis (SSA) is applied to the RMM indices for the winters of years 1979–2005. The leading pair of singular vectors are in quadrature with each other, which represents an oscillation of 40–50 days (not shown), and the two leading modes explain more than 55% of the total variance. The two principal components (PCs) of the pair are also in quadrature and the periodicity is about 40–50 days. The main steps of prediction are to predict the PCs of each mode with the autoregression model of Eq. (1) and then reconstruct the predicted values using the singular vectors and the predicted PCs. Summation of the reconstructed components of the two leading modes produces the predicted time series of RMMs (Vautard et al. 1992). The cross-validated correlation skill of the SSA-based prediction for RMM1 is shown in Fig. 5 (dotted line). For comparison, the correlation skills of the other models are also shown in the figure. The SSA-based prediction has the correlation skill of 0.5 at a lead time of ~10 days. Comparison of the previous result in Mo (2001), who forecasted the California OLR anomaly index using the SSA, reveals a similar skill score when applied to daily variables. However, the exact comparison with Mo (2001) is difficult because they used a 10–90-day filtered time series.

A comparison among the skills of various statistical models (Fig. 5) indicates that all the statistical models exhibit skill over persistence; and the best skill is produced by the simple regression model, which has prediction skill (using a correlation of 0.5 as a cutoff skill measure) to day 15 for RMMs; whereas prediction skill drops off around approximately day 10 for both the wavelet- and SSA-based models. The poor predictability of the wavelet and SSA models is due mainly to the problem of artificial tapering before the initial condition for a half-length of the time window.

3. Predictability of dynamical models

The atmospheric model used in this study is the SNU AGCM (Kim et al. 1998). This version of the model has a spectral truncation of T42 and 20 vertical levels.

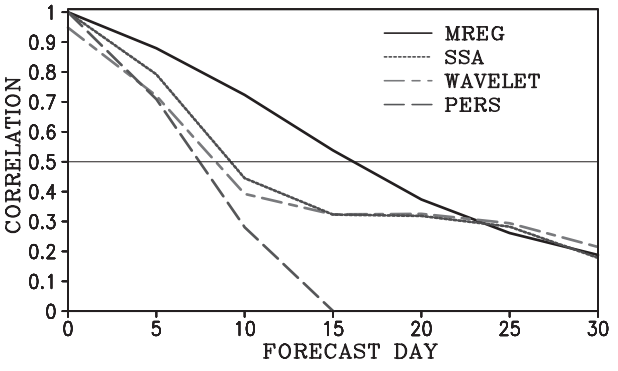

FIG. 5. Correlation skill of the SSA-based model for RMM1 (dotted line). Also plotted are the MREG (solid line), the wavelet based model (long- and short-dashed line), and persistence of the initial condition (dashed line).

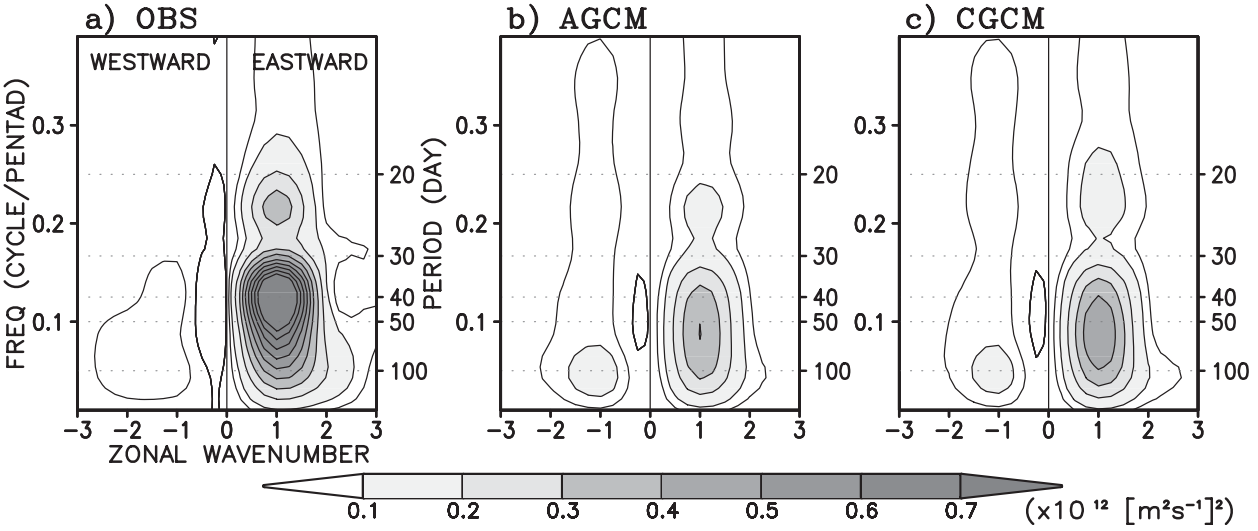

FIG. 6. Wavenumber-frequency power spectra computed with the equatorial (10°S–10°N averaged) time-longitude velocity potential at 200 hPa for the (a) observation, (b) AGCM, and (c) CGCM. Unit is 10^{12} m^4 s^{-2}.

The convective parameterization of the model is the simplified Arakawa–Schubert scheme (Moorthi and Suarez 1992). The performance of the model in simulating the MJO can be found in Waliser et al. (2003) and Kim et al. (2008a). As seen in those papers, this AGCM simulates a relatively weak MJO signal similar to most of other models, and the overall performance of this model is average compared to other models.

With this model, a climate version of serial integration similar to the NCEP Dynamical Extended Range Forecast experiment has been performed for the 27 winters of 1979–2005. In this experiment, a model prediction was made every 5 days (the so-called ''serial experiment'') and each prediction lasted for 30 days. This allows us to cover the seasonal variations of MJO predictability and to produce the same samples of prediction data as those of the statistical predictions. The initialization of AGCM prediction was made using the NCEP–National Center for Atmospheric Research (NCAR) Reanalysis 2 dataset. The serial experiments have proven to be useful in assessing the forecast skill (Schemm et al. 1996; Hendon et al. 2000; Seo et al. 2005), since the predictions cover all convection stages of MJO. The boundary condition of the AGCM is prescribed with daily varying SST, which has a persistent anomaly at the initial time, being kept same for the whole 30 days, added to the climatologically varying SST.

The SNU CGCM is also used in this study. The CGCM uses the same AGCM but is coupled with Modular Ocean Model version 2.2 (MOM2.2) oceanic GCM and the ocean mixed layer model developed by Noh and Kim (1999). Details of the SNU CGCM are documented in Kug et al. (2007). The initial ocean conditions of the CGCM are obtained with a nudging method by integrating the ocean model with the prescribed salinity and temperature fields obtained from NCEP Global Ocean Data Assimilation System (GODAS) for the recent 26 years, which covers the 26 winters of 1980–2005. The atmospheric initial conditions of the CGCM were taken from the NCEP–NCAR Reanalysis 2 dataset.

The performances of the AGCM and CGCM in simulating the MJO can be examined with long-term simulations. A long run of AGCM is performed for 27 yr with prescribed observed monthly-mean SST for 1979–2005, and the CGCM is simulated for 20 yr. Figure 6 shows the space–time power spectrum of the velocity potential at 200 hPa along the tropical belt, averaged between 10°S and 10°N. The strong spectral powers are contained in the intraseasonal time scales in the observation and in both models. But, in the model, the observed MJO time scales of 30–80 days are seen in the time scales of 40–100 days, slower than the observed, and the model intraseasonal variations are weaker than the observed. Note that the CGCM amplitudes are stronger than those of the AGCM, although those are still weaker than the observed. Details of the effect of ocean–atmosphere coupling on MJO simulation and prediction can be found in Kim et al. (2010).

The dynamical predictability of MJO can be assessed by means of the serial predictions. Figure 7 shows the prediction skills of AGCM and CGCM for RMMs. The correlation skills of RMMs for both AGCM and CGCM are similar to each other until day 20, and the CGCM skills are slightly better than those of AGCM afterward. The correlation skills of RMM1 fall to 0.5 after day 19–20 for both AGCM and CGCM. The skills for RMM2 are

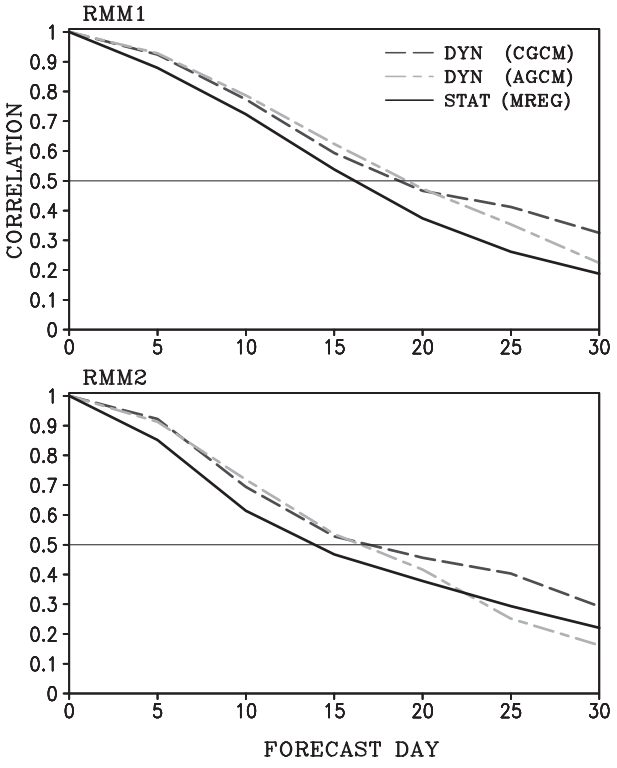

FIG. 7. Correlation skills of AGCM (long- and short-dashed line) and CGCM (dashed line) for RMM1 and RMM2 as a function of lead time, and the MREG (solid line).

a little worse than those of RMM1, as in the statistical model. As seen in Fig. 7, it is demonstrated by a fair comparison that the current dynamical predictions are better than the statistical prediction.

The similar skills of AGCM and CGCM indicate that the dynamical MJO prediction does not seem to be affected by details in the SST field. In fact, the SST anomaly produced by the coupled model is not much changed for the relatively short period of less than 30 days in the western Pacific Ocean and Indian Ocean. It is also noted that the skill of the present AGCM prediction with persistent SST anomaly is similar to the AGCM prediction with observed SST (not shown), again indicating that the MJO prediction skill of the current dynamical models comes mainly from atmospheric initial conditions and the simulation ability of the model. As indicated in previous studies (Fu et al. 2003; Fu and Wang 2004a,b; Rajendran et al. 2004; Rajendran and Kitoh 2006; Zheng et al. 2004; Fu et al. 2007; Woolnough et al. 2007), the ocean–atmosphere coupling plays an important role on MJO in terms of its activity and propagation characteristics, but the present study shows that the predictability of MJO is less sensitive to the coupling. This less sensitivity may depend on the model, and it is not ruled out that it may be due to poor representation of important processes for the coupling of the present CGCM.

4. Combination of statistical and dynamical predictions

The combination of different predictions may enhance the predictability by reducing uncertainties of the prediction models (Yoo and Kang 2005; Kang and Shukla 2006). The statistical and dynamical predictions are independent from each other, and the two dynamical prediction systems are different, although they use the same AGCM but provide a comparable prediction skill. Recently, Metzger et al. (2004) demonstrated that a multimodel ensemble can provide a better prediction skill compared to that of any individual prediction, if individual prediction schemes are independent and have a comparable skill. Therefore, it is expected to improve the prediction skill by combining those three predictions. In recent years, the multimodel ensemble predictions have been developed and implemented for weather prediction (Krishnamurti et al. 2000) and seasonal prediction (Kang and Shukla 2006). However, none of the previous studies attempt to combine the intraseasonal predictions with the dynamical and statistical models. In this study, we developed a multimodel prediction system of MJO using the best statistical model (multilinear regression) and two dynamical models and examined how the multimodel system improves the MJO prediction.

A multimodel prediction system using a standard linear regression method can be written as

$$\Psi(t)_{\text{comb}} = \beta_{t,0}\Psi(t)_{\text{stat}} + \beta_{t,1}\Psi(t)_{\text{agcm}} + \beta_{t,2}\Psi(t)_{\text{cgcm}},$$

where Ψ is the predictions and β is the weighting coefficient for each of models as a function of lead times that are obtained by a multilinear regression method. For each year prediction, the coefficients are computed with the data for the whole years except for the year of prediction. In other words, a cross-validation method is applied using the leave-out method of the prediction year to assess its predictability. Figure 8 shows the correlation skill of RMM1 for the multimodel system. For the comparison, the prediction skills are also shown for the statistical model and two dynamical predictions. Clearly, the multimodel system improves the prediction skill for the all lead times from day 1 to day 30. A correlation skill of 0.5 can be sustained until around day 23, which is about 4–5 days longer than the dynamical models and about 7 days longer than the best statistical model. A similar improvement is also obtained for RMM2 (not shown). From the result, it is suggested that the MJO predictability can be enhanced by combining many long-range

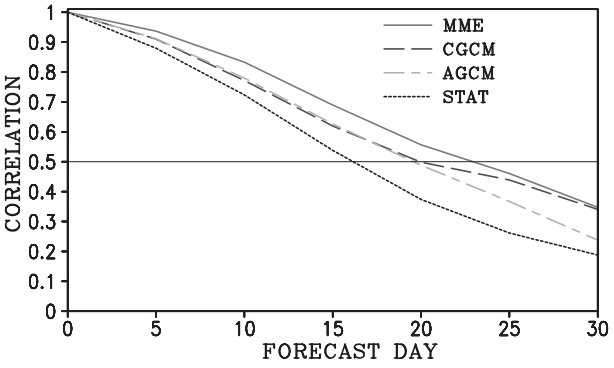

FIG. 8. Correlation skill of the multimodel ensemble (solid line), and the AGCM, CGCM, and MREG models.

forecasts. This multimodel prediction approach should be the next challenging issue for the MJO prediction.

5. Dependency of MJO predictability on the initial amplitude and phase

This section examines the dependency of initial conditions on the predictability of OLR anomalies associated with the predicted RMM indices using both statistical and dynamical models. The statistical and dynamical models chosen here are the linear regression model and the AGCM, respectively, for the 27 winters. For this purpose, the OLR anomalies (R-OLR) are reconstructed using the predicted RMM1 and RMM2 indices at each day, as described in section 2. The prediction skills are examined in this section in terms of the spatial correlation between the predicted R-OLR and the observed counterpart over the region of 15°S–15°N, 0°–300°E.

First, we examine the differences of OLR predictability for different amplitudes of initial MJO conditions. The cases are classified based on the magnitude of the square root of the sum of $(RMM1)^2$ and $(RMM2)^2$ in the domain, which is defined as ''strong'' for the magnitude larger than 2.5 (104 cases), ''moderate'' for those between 1.0 and 2.5 (392 cases), and ''weak'' for those smaller than 1.0 (125 cases). Figure 9 shows the spatial correlation skills of R-OLR for three different initial amplitudes, averaged for all cases of each category. The strong MJO certainly has a better prediction skill than that of the weak MJO, although the statistical model produces relatively bad skills after day 12–13. Interestingly, the statistical model produces a sudden decrease of the prediction skill after day 10 for the strong MJO case, whereas the skill of dynamical model decreases relatively slowly with lead times for the entire 30-day period. It is also noted that the dynamical predictability of R-OLR is better than that of the statistical model for most of lead limes, as seen in the prediction skills of the RMM indices. The present results

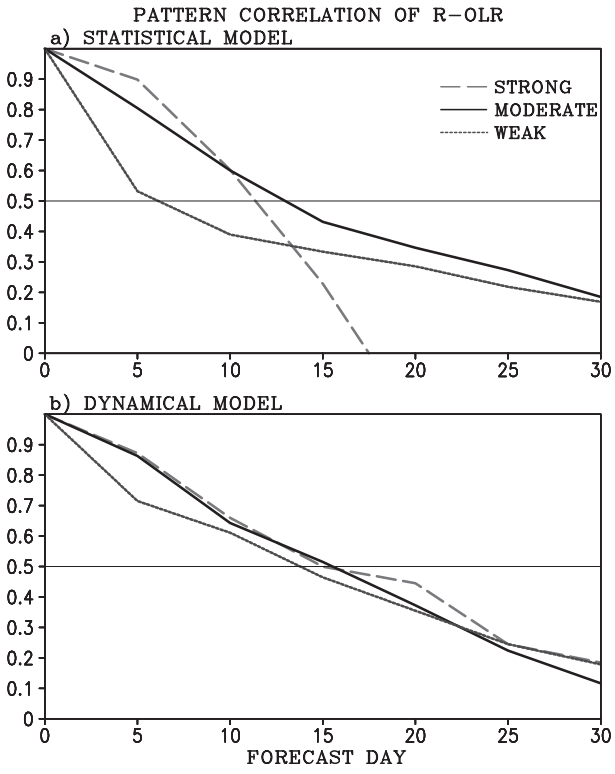

FIG. 9. Pattern correlation coefficient (for the domain of 15°S–15°N, 0°–300°E) between the predicted and verifying values of reconstructed OLR anomalies for the strong (dashed line), moderate (solid line), and weak (dotted line) MJO cases for the (a) statistical MREG model and (b) AGCM.

are consistent with the previous studies with statistical and dynamical models (Lo and Hendon 2000; Agudelo et al. 2008; Jiang et al. 2008).

The dependency of prediction skill on the initial phase of MJO is also studied in this section. As in WH04, the RMM indices are divided by eight phases that correspond to different locations of large-scale convection in the tropics. Those eight phases represent the eastward-propagating MJO phenomena reasonable well. Phase 1 corresponds to the OLR state, which represents a weak convection emerging in the western Indian Ocean and dryness prevailing over Indochina and the western Pacific Ocean. The phases of 1–4 represent the developing and eastward-propagating phases of MJO convection over the Indian Ocean. The observed OLR pattern of phase 3 is shown (Fig. 11a). The phases of 5–8 represent the decaying and eastward-propagating phases of convection over the western and central Pacific Oceans.

Figure 10 shows the characteristic of differences in the prediction skill (the spatial correlation for the domain of 15°S–15°N, 0°–300°E) for different initial phases and for different lead times. For early lead times of fewer than

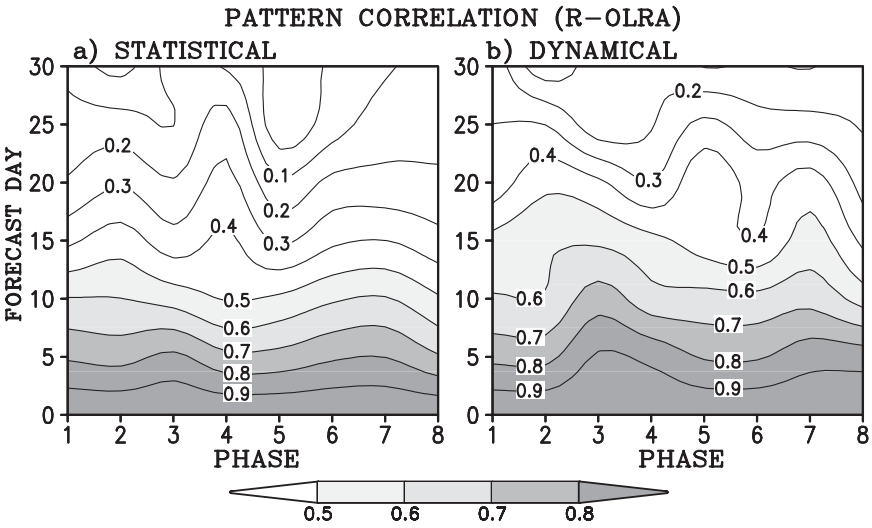

FIG. 10. Pattern correlation skill (15°S–15°N, 0°–300°E) of the reconstructed OLR anomalies as functions of different phases of MJO and forecast lead time for the (a) statistical MREG model and (b) AGCM.

15 days, the skill differences are not significant for the statistical model. Certain differences are seen in the dynamical model, which produces a relatively high skill for phases 3 and 7 (a mirror image of phase 3) and a relatively low skill for phases 1–2 and 5–6. Those skill differences are consistent with the results shown in Fig. 9, since phases 1–2 and 5–6 have relatively small MJO anomalies, whereas phases 3–4 and 7–8 have a large MJO signal in the eastern Indian Ocean and Indochina.

The time evolution of the predicted R-OLR anomalies for the eastward-propagating event is compared with those of the observation. The eastward-propagating events are selected based on the phase evolution with lead time in the observation. If three successive pentads from the initial state continue to increase the phase, then those events are classified as ''eastward-propagation event.'' Figure 11 shows the time evolution of R-OLR anomalies initiated from the initial condition of phase 3, when relatively widespread convection is present in the western Indian Ocean and Indochina. A total of 31 cases are selected for this event. Phase 3 is chosen here since the propagating characteristics is similar to but more clear than those of other phases. In the observation, the convection signal propagates eastward with amplification until day 5 and decays afterward, and dryness initiates in the eastern Indian Ocean on day 5. Afterward, the dry anomalies are intensified and propagate eastward. Both predicted OLR anomalies have similar characteristics as those of the observed. But, the predicted eastward propagation is much slower than the observed. A distinct difference between the statistical and dynamical predictions is seen in the amplitude of the anomalies, which is weaker in the statistical model than in the dynamical model. Overall, both models appear to predict the OLR anomaly patterns reasonably well up to day 20, although certain differences from the observed are seen in the amplitude and propagation speed. The slow propagation of the dynamical prediction seems to be related to the model characteristic shown in Fig. 6.

6. Summary and concluding remarks

In this paper, we assess the predictability of MJO by using various statistical and dynamical models available at present. For fair assessment and comparison, the statistical and dynamical predictions have been made using the same predictand and a similar prediction framework, particularly for the prediction interval and period. The real-time multivariate MJO (RMM) index is used as a predictand for all models.

The results of various prediction models are summarized as follows. For the predictions in various statistical models, the prediction limit of RMM1 (RMM2), which is defined as the day when the correlation decreases to 0.5, is at days 16–17 (days 14–15) for multilinear regression, and days 8–10 (days 9–12) for the wavelet- and SSA-based prediction. The multilinear regression model shows the highest prediction skill among them. The serial prediction experiments, with a similar prediction framework to those of the statistical models, have been performed using the SNU AGCM and CGCM. The prediction limit of RMMs appears at around day 20 for the CGCM and AGCM, respectively. This result demonstrates that the dynamical predictions based on SNU AGCM and CGCM

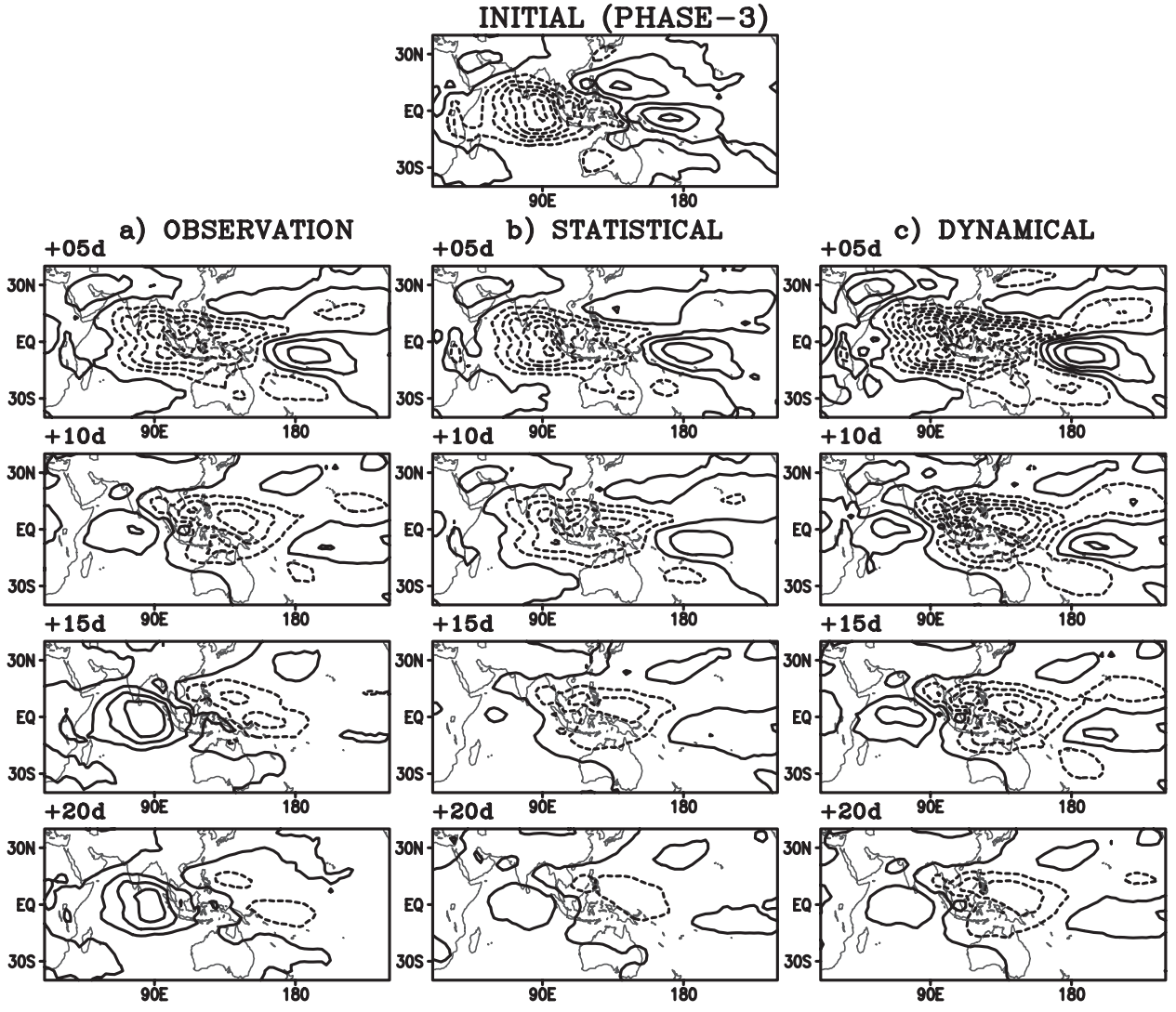

FIG. 11. Composite maps of the reconstructed OLR anomalies starting from the phase 3 initial condition for lead times from day 5 to day 20 for (a) the observation and for the predictions by the (b) statistical model and (c) AGCM, respectively. Contour interval is 4 W m^{-2}.

are better than the statistical predictions. It should be noted that the results of the statistical models could be different with the aforementioned studies based on the different forecast procedure, period, variables, and region. Moreover, the dynamical models used in this study are not the current operational forecast model, and the resolution is typical of a climate model rather than an operational forecast system; therefore, the skills of the present dynamical models may underrepresent the skill of the state-of-the-art operational system.

The statistical and dynamical predictions are combined based on a multimodel ensemble method. The multimodel prediction shows its superiority to both of the statistical and dynamical predictions over the entire forecast days. The dependency of prediction skill on the initial phase and magnitude of the MJO is investigated with both statistical and dynamical models. It is obvious that the score is better when the MJO is active than quiescent at the initial condition in both systems.

It is pointed out that those statistical models have a limitation in improving the prediction skill, while the dynamical models have a large room to improve with various ways. Optimal initialization will improve the skill, especially at the beginning of the forecasts (Vitart et al. 2007). The combination of different dynamical forecasts using multimodel ensembles also has a large potential for enhancing the prediction skill. Accordingly, the prediction skill should be reassessed continuously along with the improvement of models and the adaptation of different prediction schemes.

Acknowledgments. This work is supported by the Korea Meteorological Administration Research and Development Program under Grant CATER_2006-4206 and the second stage of the Brain Korea 21 Project.

REFERENCES

Agudelo, P. A., C. D. Hoyos, P. J. Webster, and J. A. Curry, 2008: Application of a serial extended forecast experiment using the ECMWF model to interpret the predictive skill of tropical intraseasonal variability. *Climate Dyn.,* **32,** 855–872.

Chen, T.-C., and J. C. Alpert, 1990: Systematic errors in the annual and intraseasonal variations of the planetary-scale divergent circulation in NMC medium-range forecasts. *Mon. Wea. Rev.,* **118,** 2607–2623.

Fu, X., and B. Wang, 2004a: Differences of boreal summer intraseasonal oscillations simulated in an atmosphere–ocean coupled model and an atmosphere-only model. *J. Climate,* **17,** 1263–1271.

——, and ——, 2004b: The boreal-summer intraseasonal oscillations simulated in a hybrid coupled atmosphere–ocean model. *Mon. Wea. Rev.,* **132,** 2628–2649.

——, ——, T. Li, and J. P. McCreary, 2003: Coupling between northward propagation intraseasonal oscillations and sea surface temperature in the Indian Ocean. *J. Atmos. Sci.,* **60,** 1733–1753.

——, ——, D. E. Waliser, and L. Tao, 2007: Impact of atmosphere–ocean coupling on the predictability of monsoon intraseasonal oscillations. *J. Atmos. Sci.,* **64,** 157–174.

Goswami, B. N., and P. K. Xavier, 2003: Potential predictability and extended range prediction of Indian summer monsoon breaks. *Geophys. Res. Lett.,* **30,** 1966, doi:10.1029/2003GL017810.

Hendon, H. H., B. Liebemann, M. Newman, J. Glick, and J. E. Schemm, 2000: Medium-range forecast errors associated with active episodes of the Madden–Julian oscillation. *Mon. Wea. Rev.,* **128,** 69–86.

Jiang, X., D. E. Waliser, M. C. Wheeler, C. Jones, M.-I. Lee, and S. D. Schubert, 2008: Assessing the skill of an all-season statistical forecast model for the Madden–Julian oscillation. *Mon. Wea. Rev.,* **136,** 1940–1956.

Jones, C., D. E. Waliser, W. K. Lau, and W. Stern, 2000: Prediction skill of the Madden and Julian oscillation in dynamical extended range forecasts. *Climate Dyn.,* **16,** 273–289.

——, L. M. V. Carvalho, R. W. Higgins, D. E. Waliser, and J.-K. E. Schemm, 2004: A statistical forecast model of tropical intraseasonal convective anomalies. *J. Climate,* **17,** 2078–2095.

Kang, I.-S., and J. Shukla, 2006: Dynamic seasonal prediction and predictability. *The Asian Monsoon,* B. Wang, Ed., Springer Praxis, 585–612.

——, and Coauthors, 2002: Intercomparison of the climatological variations of Asian summer monsoon precipitation simulated by 10 GCMs. *Climate Dyn.,* **19,** 383–395.

Kim, H. M., 2008: Combined and calibrated predictions of intraseasonal variation with dynamical and statistical methods. Ph.D. thesis, Seoul National University, 156 pp.

——, and I.-S. Kang, 2008: The impact of ocean–atmosphere coupling on the predictability of boreal summer intraseasonal oscillation. *Climate Dyn.,* **31,** 859–870.

——, ——, B. Wang, and J. Y. Lee, 2008a: Interannual variations of the boreal summer intraseasonal variability predicted by ten atmosphere–ocean coupled models. *Climate Dyn.,* **30,** 485–496.

——, P. J. Webster, C. D. Hoyos, and I.-S. Kang, 2008b: Sensitivity of MJO simulation and predictability to sea surface temperature variability. *J. Climate,* **21,** 5304–5317.

——, C. D. Hoyos, P. J. Webster, and I.-S. Kang, 2010: Ocean–atmosphere coupling and the boreal winter MJO. *Climate Dyn.,* doi:10.1007/s00382-009-0612-x, in press.

Kim, J. K., I.-S. Kang, and C. H. Ho, 1998: East Asian summer monsoon simulated by the Seoul National University GCM. *Proc. Int. Conf. on Monsoon and Hydrologic Cycle,* Kyongju, South Korea, Korean Meteorological Society and Amer. Meteor. Soc., 227–231.

Krishnamurti, T. N., C. M. Kishtawal, T. LaRow, D. Bachiochi, Z. Zhang, C. E. Williford, S. Gadgil, and S. Surendran, 2000: Multimodel ensemble forecasts for weather and seasonal climate. *J. Climate,* **13,** 4196–4216.

Kug, J.-S., I.-S. Kang, and D.-H. Choi, 2007: Seasonal climate predictability with tier-one and tier-two prediction systems. *Climate Dyn.,* **31,** 403–416.

Lau, K.-M., and F. C. Chang, 1992: Tropical intraseasonal oscillation and its prediction by the NMC operational model. *J. Climate,* **5,** 1365–1378.

Lo, F., and H. H. Hendon, 2000: Empirical extended-range prediction of the Madden–Julian oscillation. *Mon. Wea. Rev.,* **128,** 2528–2543.

Love, B. S., and A. J. Matthews, 2009: Real-time localised forecasting of the Madden-Julian oscillation using neural network models. *Quart. J. Roy. Meteor. Soc.,* **135,** 1471–1483.

Maharaj, E. A., and M. C. Wheeler, 2005: Forecasting an index of the Madden-oscillation. *Int. J. Climatol.,* **25,** 1611–1618.

Metzger, S., M. Latif, and K. Fraedrich, 2004: Combining ENSO forecasts: A feasibility study. *Mon. Wea. Rev.,* **132,** 456–472.

Meyers, S. D., B. G. Kelly, and J. J. O'Brien, 1993: An introduction to wavelet analysis in oceanography and meteorology: With application to the dispersion of Yanai waves. *Mon. Wea. Rev.,* **121,** 2858–2866.

Mo, K. C., 2001: Adaptive filtering and prediction of intraseasonal oscillations. *Mon. Wea. Rev.,* **129,** 802–817.

Moorthi, S., and M. J. Suarez, 1992: Relaxed Arakawa-Schubert: A parameterization of moist convection for general circulation models. *Mon. Wea. Rev.,* **120,** 978–1002.

Noh, Y., and H. J. Kim, 1999: Simulations of temperature and turbulence structure of the oceanic boundary layer with the improved near-surface process. *J. Geophys. Res.,* **104,** 15 621–15 634.

Rajendran, K., and A. Kitoh, 2006: Modulation of tropical intraseasonal oscillations by ocean–atmosphere coupling. *J. Climate,* **19,** 366–391.

——, ——, and O. Arakawa, 2004: Monsoon low-frequency intraseasonal oscillation and ocean-atmosphere coupling over the Indian Ocean. *Geophys. Res. Lett.,* **31,** L02210, doi:10.1029/2003GL019031.

Schemm, J. K.-E., H. Van den Dool, and S. Saha, 1996: A multi-year DERF experiment at NCEP. Preprints, *11th Conf. on Numerical Weather Prediction,* Norfolk, VA, Amer. Meteor. Soc., 47–49.

Seo, K. H., J. K. E. Schemm, C. Jones, and S. Moorthi, 2005: Forecast skill of the tropical intraseasonal oscillation in the NCEP GFS dynamical extended range forecasts. *Climate Dyn.,* **25,** 265–284.

Slingo, J. M., and Coauthors, 1996: Intraseasonal oscillations in 15 atmospheric general circulation models: Results from an AMIP diagnostic subproject. *Climate Dyn.,* **12,** 325–357.

Torrence, C., and G. P. Compo, 1998: A practical guide to wavelet analysis. *Bull. Amer. Meteor. Soc.,* **79,** 61–78.

Vautard, R., P. Yiou, and M. Ghil, 1992: Singular-spectrum analysis: A toolkit for short, noisy chaotic signals. *Physica D,* **58,** 95–126.

Vitart, F., S. Woolnough, M. A. Balmaseda, and A. M. Tompkins, 2007: Monthly forecast of the Madden–Julian oscillation using a coupled GCM. *Mon. Wea. Rev.,* **135,** 2700–2715.

Waliser, D. E., C. Jones, J.-K. E. Schemm, and N. E. Graham, 1999a: A statistical extended-range tropical forecast model based on the slow evolution of the Madden–Julian oscillation. *J. Climate,* **12,** 1918–1939.

——, K. M. Lau, and J.-H. Kim, 1999b: The influence of coupled sea surface temperatures on the Madden–Julian oscillation: A model perturbation experiment. *J. Atmos. Sci.,* **56,** 333–358.

——, and Coauthors, 2003: AGCM simulations of intraseasonal variability associated with the Asian summer monsoon. *Climate Dyn.,* **21,** 423–446.

Webster, P. J., and C. Hoyos, 2004: Prediction of monsoon rainfall and river discharge on 15–30-day time scales. *Bull. Amer. Meteor. Soc.,* **85,** 1745–1765.

——, and Coauthors, 2002: The JASMINE pilot study. *Bull. Amer. Meteor. Soc.,* **83,** 1603–1629.

Wheeler, M., and H. Hendon, 2004: An all-season real-time multivariate MJO index: Development of an index for monitoring and prediction. *Mon. Wea. Rev.,* **132,** 1917–1932.

Woolnough, S. J., J. M. Slingo, and B. J. Hoskins, 2000: The relationship between convection and sea surface temperature on intraseasonal timescales. *J. Climate,* **13,** 2086–2104.

——, F. Vitart, and M. A. Balmaseda, 2007: The role of the ocean in the Madden-Julian oscillation: Implications for MJO prediction. *Quart. J. Roy. Meteor. Soc.,* **133,** 117–128.

Wu, M. L., S. Schubert, I.-S. Kang, and D. Waliser, 2002: Forced and free intraseasonal variability over the South Asian monsoon region simulated by 10 AGCMs. *J. Climate,* **15,** 2862–2880.

Yoo, J. H., and I.-S. Kang, 2005: Theoretical examination of a multi-model composite for seasonal prediction. *Geophys. Res. Lett.,* **32,** L18707, doi:10.1029/2005GL023513.

Zheng, Y., D. E. Waliser, W. Stern, and C. Jones, 2004: The role of coupled sea surface temperatures in the simulation of the tropical intraseasonal oscillation. *J. Climate,* **17,** 4109–4134.